



Research papers

Dramatic typhoon-induced variability in the grain size characteristics of sediments at a meso-macrotidal beach

Binbin Ma^a, Zhijun Dai^{a,b,*}, Wenhong Pang^a, Zhenpeng Ge^a, Shushi Li^b, Xuefei Mei^a,
Hu Huang^{b,**}

^a State Key Laboratory of Estuarine and Coastal Research, East China Normal University, Shanghai, 200062, China

^b The Key Laboratory of Coastal Science and Engineering, Beibu Gulf University, Qinzhou, 535011, China



ARTICLE INFO

Keywords:

Sediment grain size
Variability
Typhoon Rammasun
Yintan Beach
Change pattern
Influencing factor

ABSTRACT

Knowledge of sediment grain size characteristics is important for a better understanding of the morphodynamic behavior of beaches worldwide. In this paper, dramatic changes in the grain size of sediments at Yintan Beach, South China in response to Typhoon Rammasun (tropical storm no. 1409) were analyzed on the basis of the collected sediments, beach elevation, and hydrological data from June 1 to July 31. Variations in beach geomorphology were interpreted using the digital elevation taken by LiDAR technology, while changes in sediment grain size were detected by sediment parameters and associated sediment components. The results show that the sediments of Yintan Beach were nearly pure sand before Rammasun and became coarser and slightly better sorted with a higher negative skew after Rammasun. The sediment grain size pattern shifted from a high content (39%) of very fine sand in the lower intertidal zone pre-Rammasun to a high content (76%) of fine sand in the swash zone post-Rammasun. During Rammasun, wave action was responsible for the main transition of grain size pattern in the lower intertidal and mid-tidal zones, and tidal level and beach morphology could affect the grain size distribution of the sandbar and trough in the swash zone. In addition, the increase in the coarse-grained fraction in the upper beach and berm was primarily due to wind action.

1. Introduction

Beaches, constituting one of the most valuable coastal landforms, act as the first barrier against the hydrodynamic forces of waves and currents. However, beaches around the world face great challenges due to storm-induced erosion and relative sea-level rise (Nicholls and Cazeau, 2010). Therefore, it is of significant importance to detect beach variabilities in response to extreme storm activities.

In recent decades, investigations regarding different morphodynamic states under the impacts of storm actions have been conducted worldwide (Moore et al., 1999; Aagaard et al., 2005; Burvingt et al., 2017). It has been found that both erosion and progradation are prevailing conditions during high-energy storms (Costas et al., 2005; Stockdon et al., 2009; Anthony, 2013). The beach in Duck, North Carolina suffered dominant offshore sediment transport-induced erosion during a storm event (Conley and Beach, 2003). On the Mississippi mainland coast, the backshore areas of East Belle Fontaine Beach

prograded 3–7 m and aggraded 20–90 cm at several locations after Hurricane Georges (Otvos, 2004). In addition, the impacts of storms on cross-shore bar mobility in intertidal bar-trough systems at beaches have also been widely researched (Masselink et al., 2006; Dai et al., 2007, 2008; Sedrati, 2007).

Meanwhile, Dissanayake et al. (2015) documented that successive small storms that occur at close intervals generally lead to increased damage compared to large isolated storms because the clusters prevent beach system recovery. Lee et al. (1998) found that beach recovery may take a period from days to even years, which is based on the hydrodynamic regime and sediment budget conditions. Moreover, Grottoli et al. (2017) demonstrated that the beach recovery period may not be determined by the degree of morphological variations caused by storms. As the dominant remote sensing technique, LiDAR has been widely used in earth science research (Stockdon et al., 2009; Tang et al., 2014; Keijpers et al., 2014), is characterized by high accuracy and resolution and is capable of accurately quantifying morphological variability caused by

* Corresponding author. State Key Lab of Estuarine and Coastal Research, East China Normal University, Shanghai, China.

** Corresponding author. The Key Laboratory of Coastal Science and Engineering, Beibu Gulf University, Qinzhou, China.

E-mail addresses: zjdai@sklec.ecnu.edu.cn (Z. Dai), mrhuanghu@126.com (H. Huang).

storms (Durán et al., 2016). Based on this technique, Ge et al. (2017) demonstrated that there were two transition points during the process of Yintan Beach recovery on the South China coast, thereby dividing the recovery into three stages.

Various kinds of factors are crucial in how storms impact beaches. The extent of beach damage is generally dominated by water level, storm duration, wave direction and peak wave period, and greater damage is usually caused by large storm events that cause high waves (Karunaratna et al., 2014; Cox and Pirrello, 2001). Russell (1993) noted that the sediment transport direction along beaches is generally impacted by a combination of three factors—wave velocity asymmetry, oscillatory infragravity waves and undertow—which cause onshore and offshore transport. The wave velocity, which causes sediment transport, is related to the sediment grain size and sorting (McLaren and Bowles, 1985). Meanwhile, simulation of the beach profile evolution is substantial based on the sediment grain size distribution across beaches (Gallagher et al., 1998). However, most hydrodynamic and morphologic coastal modelers assumed that beaches were composed of homogeneous and well-sorted sand, which deviates from reality (Gallagher et al., 2011; Gunaratna et al., 2019). The consideration of heterogeneous sediment behavior has been suggested to improve the coastal morphology simulation in many studies (Bascom, 1951; Moutzouris, 1989; Dai et al., 2010). Thus, sediment grain size characteristics of beaches still need to be broadly discussed.

Granulometric analysis of the unconsolidated sediments of beaches reveals that sediments usually exhibit significant changes both in space and in time. Grain size data were used as indicators to identify depositional environments (beaches, dunes, riverbeds, etc.) in early studies (Friedman, 1961, 1967; 1979; Visher, 1969). Moutzouris (1989) found that grain size segregation is more evident in the cross-shore direction than in the longshore direction. The sediment grain size distribution is dependent on the sediment source, transport mechanism and location in both the cross-shore and longshore direction (Abuodha, 2003).

Furthermore, sediment grain size is related to morphodynamic response because the grain size variation is usually related to the location of the sediments in a rip current cell. In general, larger grain sizes usually exist in areas where high-energy dissipation occurs, while smaller ones emerge elsewhere (Gallagher et al., 2016). In addition, an empirical orthogonal function (EOF) method has been used to better understand the grain size distribution in differential energy zones (Liu and Zarillo, 1989) and their response to the relative sea level rise (Zhang et al., 2014).

Although some studies have paid attention to the variability in sediment grain size characteristics in response to storm activities, this topic is far from fully understood. We carried out a study on sediment grain size characteristic variability in Yintan Beach (a meso-macrotidal beach) in response to Typhoon Rammasun. In this study, terrain data and sediment samples in a typical region of Yintan Beach were collected before and after Typhoon Rammasun. The aims of this paper are as follows: 1) examine the variability in sediment grain size characteristics at Yintan Beach before and after Typhoon Rammasun; 2) reveal the change in the variable pattern of the sediment grain size; and 3) identify the driving forces affecting the variability in sediment grain size.

2. Physical setting

Yintan Beach, located on the northern coast of Beihai Gulf and open to the South China Sea, is a meso-macrotidal beach (Fig. 1). The beach is approximately 13 km in length, and the shoreline is approximately 155° oblique to the latitudinal direction. Diurnal and irregular semidiurnal tides along Yintan Beach alternate over spring and neap, respectively. The maximum spring tidal range can reach 5.36 m, while the mean spring tidal range is 3.6 m. The beach is further divided into five areas, namely, the upper beach, berm, swash zone, mid-tidal zone and lower intertidal zone in the cross-shore direction, according to the local tide level in this study (Fig. 1). The mean spring tidal current velocity of the

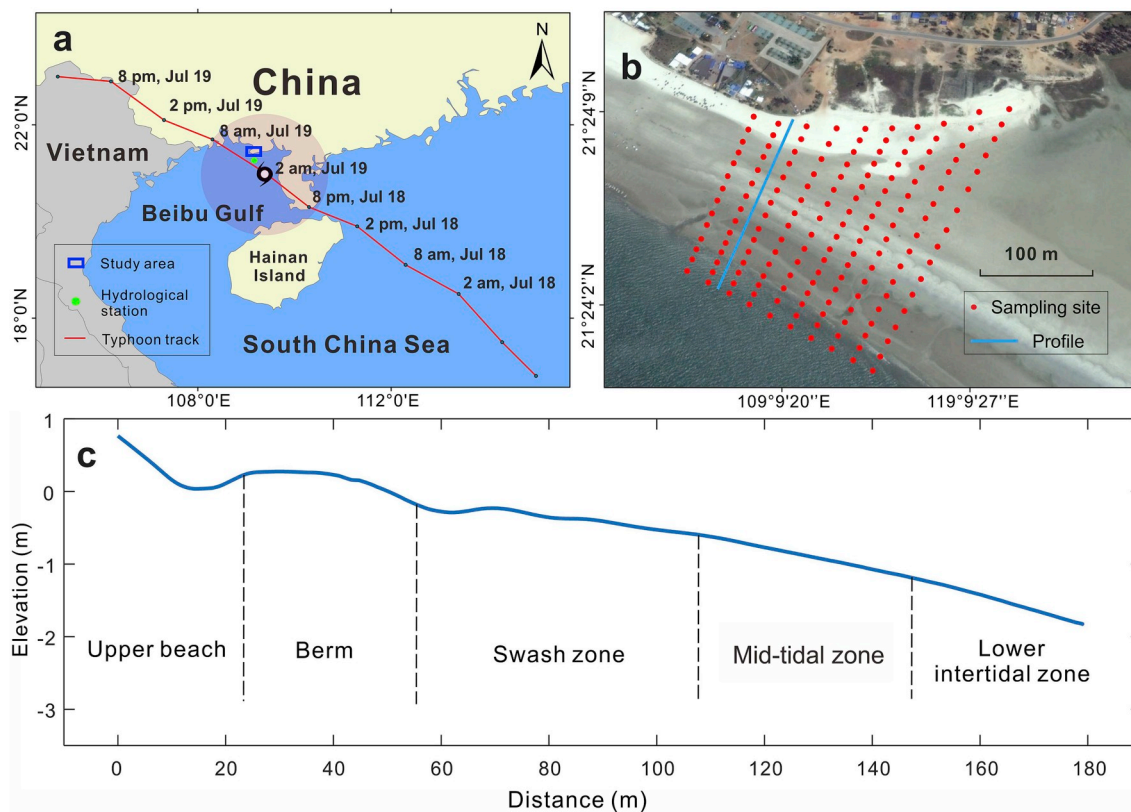


Fig. 1. (a) Map of Yintan Beach, with the Rammasun track and hydrological stations; (b) Surface sediment sampling sites and transect location (image from Google Earth); (c) Schematic profiles of the upper beach, berm, swash zone, mid-tidal zone and lower intertidal zone across the transect.

flood tide is 0.13 m/s, while that of the ebb is 0.31 m/s (Huang et al., 2011). Meanwhile, under the impacts of monsoons, the SSW wave direction in summer changes to a NNE wave direction in winter. The mean wave height in this region is approximately 0.5 m (Zhou et al., 2015). Moreover, it is a common feature for alongshore multibar patterns to be distributed at the center of the beach.

In summer and autumn, the familiar typhoon, which is a type of tropical cyclone, can influence beaches through violent winds, waves and storm surge in local areas. Typhoon Rammasun (tropical storm no. 1409) was the strongest typhoon to pass over the Beibu Gulf since 1949. It generated in the Northwest Pacific Ocean on July 12, 2014 (GMT+8), and then moved toward South China in the northwest direction (Fig. 1). The wind speed increased from an initial value of 18 m/s in the Pacific Ocean to a peak value of 72 m/s in Beibu Gulf on July 18th, 2014 (GMT+8) (Ying et al., 2014). Thereafter, the violent typhoon caused great damage to the study area when it passed over Beihai on July 19 (Fig. 2) then gradually dissipated in Yunnan on July 22, 2014.

3. Materials and methods

3.1. Hydrological data collection

There is an offshore hydrological station governed by the State Oceanic Administration of China (SOA), which is approximately 30 km away from the study area (Fig. 1). The hourly water level was measured by a buoy, while the wave height, wave period and wave direction were measured by a visual observation method. The field operator recorded the maximum wave height, the maximum wave period and the wave direction at four given times (8 a.m., 11 a.m., 2 p.m. and 5 p.m.) on each day, which was determined by the SOA. Therefore, we downloaded the hydrological data of the study area from June 1 to July 31 from the China Oceanic Information Network (<http://www.nmdis.org.cn/>).

3.2. Beach morphology scanning

To detect morphological changes caused by Rammasun, a 3D terrestrial laser scanner (RIEGL-VZ4000) (http://www.riegl.com/uploads/tx_pxpriegldownloads/

RIEGL_VZ-4000_Datasheet_2017-09-01.pdf) was used to measure Yintan Beach morphology before and after Rammasun typhoon. The laser scanner acquired original scan position data operating at 200 kHz. Data of the study area from two scan positions were collected before and after the typhoon. Then, the data were adjusted to the Beijing-54

coordinate system and national height datum 1985 of China with the RISCAN PRO software. There were approximately 516 laser points per square meter within 150 m of the scan position that were used to guarantee high resolution and accuracy. Thereafter, the digital elevation models (DEMs) before and after Rammasun were built in ArcGIS 10.2 based on the point-cloud dataset. The DEM has a high vertical and horizontal resolution of 5 cm and high accuracy, and the measuring error was controlled within 20 mm (Ge et al., 2017). Finally, the beach morphology changes in response to Rammasun were detected by a difference analysis of the two DEMs.

3.3. Beach sediments sampling and analysis

To understand the sediment dynamic process before and after Rammasun, 162 sediment samples along 10 transects of the beach were collected (on July 12 and 20, 2014) (Fig. 1). All the sediment samples were taken nearly 1–2 cm below the beachface. The interval between the two adjacent transects was approximately 30 m, while two adjacent sediment sites in one transect had an interval of approximately 15 m.

In the laboratory, salt absorbed on the sediments was leached, and then the grain size analysis of each sediment sample was conducted by a multifunctional particle size analyzer (Camsizer XT), which is the most advanced dynamic digital imaging particle size analyzer. Designed by Retsch Technology in Germany based on ISO13322-2, Camsizer XT is characterized by dual CCD imaging technology, with B-CCD recording the size and shape of large particles and Z-CCD recording those of small particles (Anonymous, 2013). Moreover, Camsizer XT is the optimal analyzer to analyze the particle size of Yintan Beach sediments, as it can obtain detailed data and reveal fine differences in the particle sizes in space and in time.

Based on the measurements of each sample, the parameters of the mean grain size (μ), sorting coefficients (σ) and skewness (SK) were calculated by the statistical moment method (McManus, 1988). The sediment components of all samples were strictly calculated according to the particle size distribution classification scheme, which was released by the academic authority — American Geophysical Union (Lane, 1947). Then, the spatial distributions of the grain size parameters and components before and after Rammasun were analyzed. Moreover, to detect the changes in grain size parameters and components in the five zones, a comparison of the parameters and components in a typical transect (the third transect) before and after Rammasun was made.

4. Results

4.1. Variations in the nearshore hydrological conditions

There were eight other tropical cyclone tracks that were generated before Rammasun in 2014 in the Asia-Pacific region (Auxiliary material, Fig. S1). Rammasun was the first tropical cyclone that passed over the study area in 2014, and none of the other cyclones affected the study area before Rammasun. Furthermore, the annual mean significant wave height each month was no more than 1 m, while the mean wave period was less than 4 s (Auxiliary material, Fig. S2). Therefore, the beach state before Rammasun can be regarded as an accurate representation of fair-weather conditions.

Fig. 3a shows the hourly water level and storm surge level in the nearshore zone from June 1 to July 31, covering approximately four and a half lunar tidal cycles. It can be seen that the minimum and maximum water levels, which occurred during the spring tide period, reached 58 cm and 518 cm, respectively (the depth reference is the Yellow Sea datum of China). Typhoon Rammasun arrived at the study area at the beginning of the neap tide on July 19. The storm caused an obvious small surge (red line) with a maximum amplitude of nearly 170 cm. During the storm surge, the maximum water level reached 392 cm in the study area (Fig. 3a).

Before Rammasun, the daily maximum wave height ranged from 0.3



Fig. 2. Rammasun caused severe damage to Yintan Beach, including a (a) signpost that fell into the road; (b) almost all branches of a tree being broken; (c) a gate and sentry box that were blown down; and (d) a tree that collapsed from the root. (Photo time: July 20th, 2014).

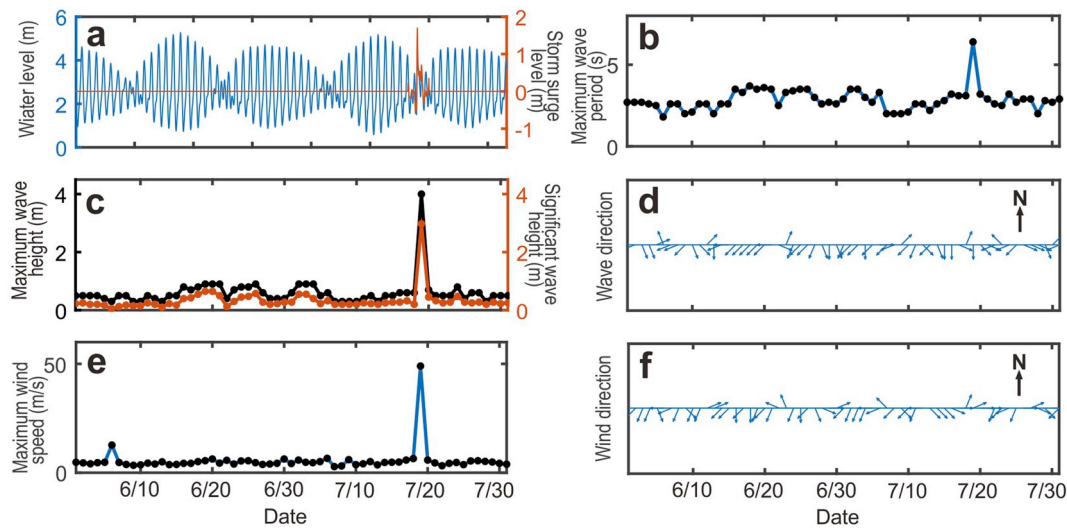


Fig. 3. Hydrological regime in the study area during June 1 - July 31: (a) observed hourly water level and storm surge level; (b) daily maximum wave period; (c) daily maximum wave height and significant wave height; (d) daily wave direction; (e) daily maximum wind speed; and (f) daily wind direction.

to 0.9 m, while the significant wave height ranged from 0.2 to 0.6 m. The daily maximum wave period varied from 1.8 to 3.5 s, and the dominant wave direction was southwesterly from June 1 to July 18 (Fig. 3b, c and 3d). There were no waves greater than 1 m in the preceding 48 days before Typhoon Rammasun. The daily maximum wind speed from June 1 to July 18 varied from 3.1 to 12.7 m/s, and the dominant wind direction was southwesterly and southeasterly. On July 19, when the typhoon began to impact Yintan Beach, the maximum wind speed was approximately 50 m/s with an ENE wind direction (Fig. 3e and f). At the same time, the maximum wave height in the local sea area increased to 4 m, and the significant wave height rose to 3 m with the dominant wave direction turning to the south, and the maximum wave period reached 6.4 s (Fig. 3b, c and 3d). After Rammasun, the maximum wind speed on July 20 immediately decreased to 5.8 m/s, while the maximum wave height decreased to 0.7 m with the dominant wave direction returning to the southwest, and the maximum wave period declined to 3.2 s (Fig. 3b, c and 3d).

4.2. Beach morphological changes

There were clearly morphological changes in Yintan Beach following Rammasun making landfall. Two separate sandbars were found in the swash zone, where the sandbar crests were nearly parallel with the shoreline before Rammasun (Figs. 4a and 5a). However, under the impacts of Rammasun, sediments infilled the channel between the previous sandbars so that the 2 bars transformed into one larger sandbar after the typhoon, with the ridge presenting a slightly crooked configuration and a relatively flat swash zone along the beachface (Figs. 4b and 5b).

Meanwhile, the distribution of slope degree along the Yintan Beach is shown in Fig. 6. Before Rammasun, the beach slope was approximately

1.5° in the lower intertidal zone, and quite steep in the toe of the sandbars. The rest of the beach was almost flat ($<0.5^\circ$) (Fig. 6a). However, the impact of Rammasun generated dramatic changes in the beach slope. Due to the variation in the previous two sandbars, the steep slope in the toe of the sandbars disappeared, while in the lower intertidal zone, the slope was steeper ($>2^\circ$) than it was before Rammasun (Fig. 6b).

Furthermore, although slight erosion and accretion (ranging from -2 cm to 2 cm) were observed alternatively in most of the study area, there were severe erosion (<-6 cm) and accretion (>6 cm) zones. Specifically, the area with over 10 cm of erosion existed in the lower intertidal zone, whereas the area with accretion intensity approaching 25 cm was detected in the previous toe of the sandbars (Fig. 6c).

4.3. Variations in sediments grain size

4.3.1. Grain size parameters before Rammasun

Based on the of sediment sample measurements on July 12, it can be found that there were clearly distinct characteristics in the grain size parameters from the upper beach to the lower intertidal zone (Fig. 7). Fig. 7a indicates that the distribution of the mean grain size (μ) before Rammasun ranged from 2.1ϕ to 3.0ϕ . The coarse fraction (2.1ϕ) existed in the upper beach around the backshore dune, while the relatively fine fraction (3.0ϕ) was distributed over the lower intertidal zone. In addition, in the third transect, the mean grain sizes in the five zones from the upper beach to the lower intertidal zone were approximately 2.4ϕ , 2.4ϕ , 2.5ϕ , 2.6ϕ and 2.8ϕ (Fig. 8a). This means that the mean grain size (μ) increased from the upper beach to the lower intertidal zone, suggesting that the surface sediment grain size became finer in the seaward direction.

The distribution of the sorting coefficient (σ) before Rammasun ranged from 0.37 to 0.85 (Fig. 7c). The better sorting fraction with a relative low value (nearly 0.4) emerged in the swash zone where the sandbar was located, while the relatively worse sorting fraction was located in the upper beach and lower intertidal zone. This means that sediments sorting improved from upper beach to the swash zone and worsened from the swash zone to the lower intertidal zone in the seaward direction, which is consistent with Fig. 8b.

Meanwhile, Fig. 7e shows that the distribution of skewness before Rammasun ranged from -0.31 to 0.08. The sediments skewness in the lower intertidal zone presented a negative value, which suggested the concentration of the fine-grained fraction, while in the swash zone and berm, the skewness almost approached zero, indicating that the



Fig. 4. The alongshore sandbars at Yintan Beach before and after Rammasun. (a) Photo taken on July 18, 2014; (b) photo taken on July 20, 2014.

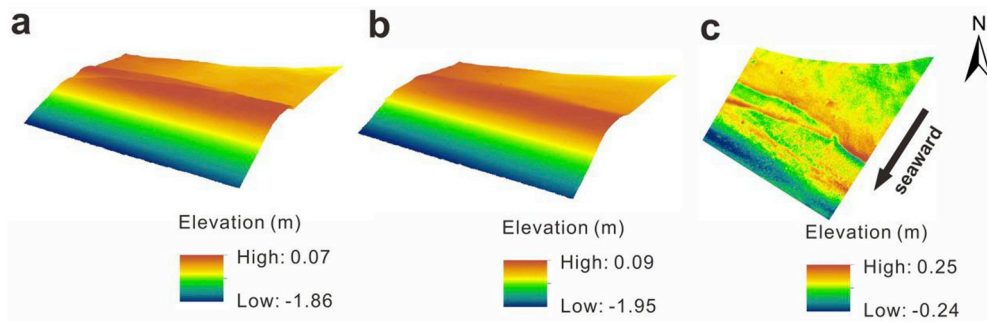


Fig. 5. Distribution of slope degrees at Yintan Beach (a) before Rammasun and (b) after Rammasun.

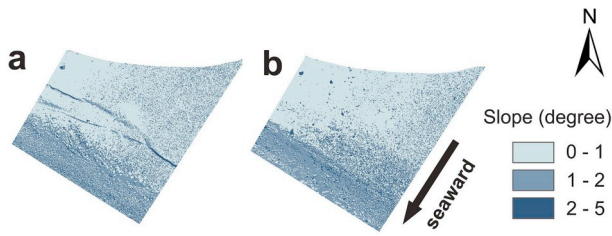


Fig. 6. 3D morphological changes in Yintan Beach before and after Rammasun. (a) Before Rammasun; (b) after Rammasun; (c) erosion and accretion evolution.

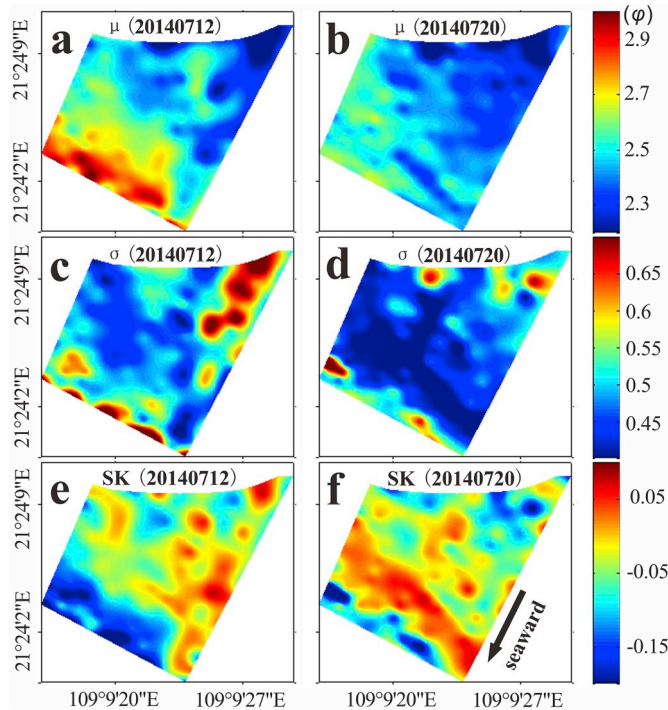


Fig. 7. Distributions of sediment grain size parameters. (a) Mean grain size before Rammasun; (b) mean grain size after Rammasun; (c) sorting coefficient before Rammasun; (d) sorting coefficient after Rammasun; (e) skewness before Rammasun; (f) skewness after Rammasun.

sediment frequency nearly followed a Gaussian distribution (Fig. 8c). In addition, positive skewness was detected in the two transects in the eastern part of the study area.

4.3.2. Grain size parameters after Rammasun

It can be revealed that the distribution of the mean grain size (μ) ranged from 2ϕ to 2.7ϕ based on the measurement of samples on July

20, indicating that the surface sediment generally became coarser after Rammasun (Fig. 7b). The coarse fraction (2ϕ) still located in the upper beach area around the backshore dune, while the fine fraction in the lower intertidal zone turned to be 2.7ϕ , which was coarser than that before Rammasun. Moreover, the mean grain sizes in the five zones of the third transect were approximately 2.3ϕ , 2.3ϕ , 2.4ϕ , 2.5ϕ and 2.6ϕ from the upper beach to the lower intertidal zone, which indicated that the mean grain size of sediments along the beach was generally larger after Rammasun (Fig. 8a). In total, the mean grain size (μ) became larger from the upper beach to the lower intertidal zone, while the grain size generally turned coarser after Rammasun.

The distribution of sorting coefficient (σ) after Rammasun ranged from 0.35 to 0.7 (Fig. 7d). The better sorting fraction with a relatively low value emerged in the swash zone where the sandbar was located. The mean value of the sorting coefficient in both the swash zone and mid-tidal zone was approximately 0.4, which was obviously lower in comparison with that during the pre-Rammasun stage. In general, post-Rammasun sediments on the beach were mostly better sorted than those before Rammasun, while the sorting was better sorted from the upper beach to the swash zone and worsened from the swash zone to the lower intertidal zone in the seaward direction (Fig. 8b).

In addition, the distribution of skewness after Rammasun also changed obviously. Fig. 7e shows that the skewness ranged from -0.35 to 0.07 . In the third transect, sediment skewness mostly increased after the typhoon in these zones on the beach except for the berm, indicating an increase in the percent of the coarse-grained fraction (Fig. 8c). The area with zero skewness sediments shifted from the swash zone and berm to the mid-tidal zone. In the lower intertidal zone and upper beach, sediment skewness was still negative, but increased to -0.06 and -0.08 (Fig. 8c).

4.4. Variations in sediment components

4.4.1. Distribution of sediment components before Rammasun

Sediments on Yintan Beach are composed of sand and silt, and we further divided the samples into nine components, ranging from very fine silt to very coarse sand (Fig. 9). The max silt component content was less than 3% before Rammasun, and the mean sand component content was more than 98% (Table 1), which indicates that sediments of Yintan Beach is nearly pure sand.

Furthermore, very fine sand (VFS), fine sand (FS) and medium sand (MS) accounted for 19%, 63% and 15% respectively, of the sediments (Table 1). In the third transect, it can be found in Fig. 8a that the VFS content of the berm was lower than that of the upper beach, while it was higher in the seaward direction from the berm to the lower intertidal zone. Meanwhile, the FS content of the berm was higher than that of the upper beach and lower from the berm to the lower intertidal zone (Fig. 8b). There was no significant spatial variation pattern in the MS fraction content, which exhibited the highest value at the berm (Fig. 8c).

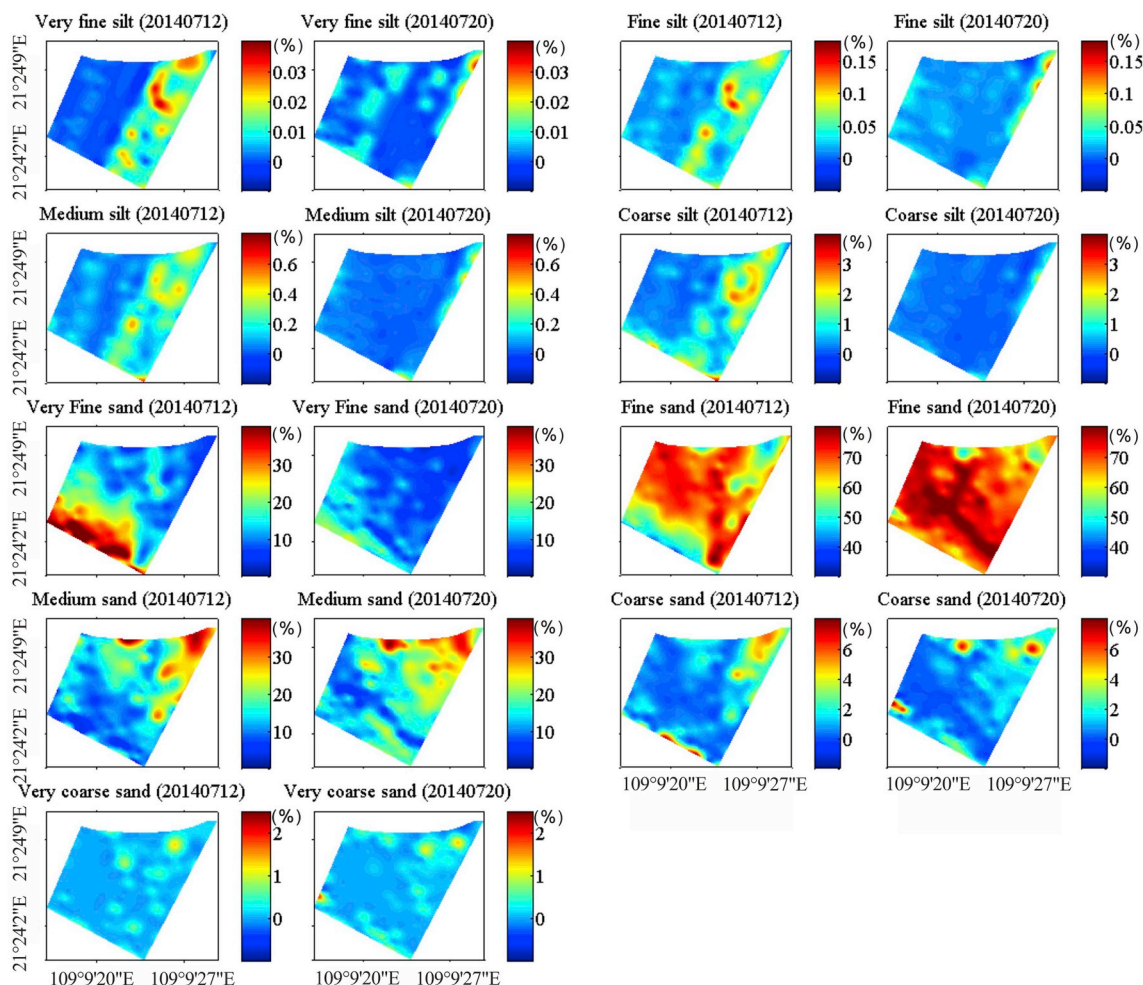


Fig. 8. Spatial distributions of sediment components before and after Rammasun.

4.4.2. Distribution of sediment components after Rammasun

With the impact of Rammasun the mean silt component content decreased to 0.46% (Table 1). In contrast, the mean sand component content increased to 99.54%, which was more than that before Rammasun. This indicated that the sediments of Yintan Beach transformed into purer sand after Rammasun.

Moreover, dramatic variations in the distribution of the beach sediment components were discovered. There was a significant decrease in the VFS fraction (Fig. 9), especially in the lower intertidal zone of the third transect, where the content decreased from 39% during pre-Rammasun to 17% during post-Rammasun, and the mid-tidal zone, where the content decreased from 28% to 12% (Fig. 8a). Instead, the content of the FS fraction in the lower intertidal and mid-tidal zones increased from 49% to 70% and from 58% to 76%, respectively. In addition, in the upper beach around the backshore dune, an increase in the MS fraction and a decrease in the coarse sand (CS) fraction were observed (Fig. 9). In general, the distribution pattern of beach sediment components changed greatly compared to that before Rammasun. Specifically, the VFS fraction and FS fraction in the five zones were distributed more uniformly (Fig. 8a and b). The MS fraction content decreased from the upper beach to the swash zone, but increased from the swash zone to the lower intertidal zone in the seaward direction. The fractions of coarse sand and very coarse sand both accounted for a small proportion. In summary, the changes in the composition of sediment implied a coarsening process in the sedimentary environment due to Rammasun induced changes in dynamic action.

5. Discussion

Although grain size analysis is a traditional method, it can clearly reveal the sensitivity of grain size parameters and composition in different zones of the beach in response to typhoons. In addition, the combination of traditional methods and LiDAR technology can deepen our understanding of beach processes in extreme events and promote the development of beach morphodynamics. Here, we explore the dominant influencing factors in the following four aspects.

5.1. Impact of tide level

The tide level during the peak of the storm plays an important role in modifying the local coastal sedimentary environment, as it can affect the range of storm impact. Storm events that occur during astronomical tide are usually one of the main reasons why beaches experienced serious erosion and shoreline retreat over almost the entire beach length, such as along the European Atlantic coasts (Anthony, 2013; Masselink et al., 2016; Burvingt et al., 2017). However, Rammasun hit Yintan Beach during a neap tide period (Fig. 3a). Rammasun arrived at the beginning of neap tide on July 19 and caused a short-term surge, when the water level was lower than the mean high water level of the spring tide. Consequently, the surge energy was not as sufficient as that along the European Atlantic coasts, and only generated slight beach erosion, with a peak intensity of erosion less than 0.25 m (Fig. 6c).

Due to the neap tide level during Rammasun, the sediment grain size characteristics in the lower intertidal, midtidal and swash zones changed

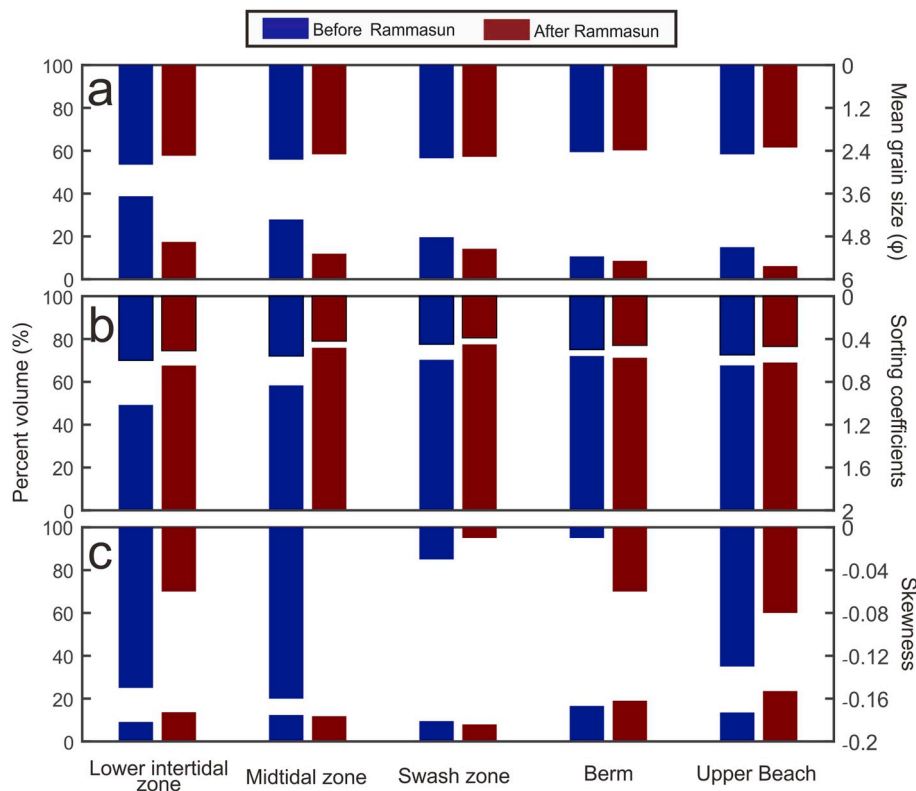


Fig. 9. Comparison of grain size parameters and components before and after Rammasun. (a) Percent volume of very fine sand (bottom) and mean grain size (top); (b) percent volume of fine sand (bottom) and mean grain size (top); (c) percent volume of medium-size sand (bottom) and skewness (top).

Table 1
Mean percentage of each component of silt and sand before and after Rammasun.

	Mean silt content (%)				Mean sand content (%)				
	Very fine silt	Fine silt	Medium silt	Coarse silt	Very fine sand	Fine sand	Medium sand	Coarse sand	Very coarse sand
Before Rammasun	1.79				98.21				
	0.01	0.05	0.24	1.49	18.57	63.02	15.09	1.39	0.14
After Rammasun	0.46				99.54				
	0.00	0.03	0.09	0.34	10.84	70.62	16.77	1.17	0.14

more dramatically than that in the berm and upper beach (Fig. 7). The variability in the mean grain size was most significant in the lower intertidal zone where intense erosion also occurred (Fig. 7a and b). Compared to the lower intertidal zone, the mean grain size in the berm and upper beach showed little change. Hence, the variations in the sediments grain size characteristics of Yintan Beach were inhomogeneous. In general, when the wave action imposed on the water level reached the swash zone, i.e., the farthest area it can affect, the tide level controlled the beachface evolution.

5.2. Impact of wave action

Storm-induced significant beach variation can generally be attributed to hydrodynamic forcing, such as wave, tide and storm surge forcing (Loureiro et al., 2012). Usually, the distribution of sediment grain size reflects hydrodynamic variation (Friedman, 1979). The waves become unstable and break in the breaking zone; thereafter, there is a sequence of swash run-up and run-down, which is accompanied by the dissipation of wave energy. Hence, wave action is undoubtedly the dominant factor that affected the sediment grain size characteristics of Yintan Beach during Rammasun.

Under fair-weather conditions, due to the wave asymmetry breaking in shallow water, the onshore motion is both longer and stronger than

the offshore motion (Pang et al., 2019). As a consequence, onshore sediment transport is higher than offshore transport, while the wave-orbital motion stirs the sediments back and forth in the bed. Sand is thereby aggraded along the shoreline, and the beach is effected by this mechanism (Dronkers, 2005). There are usually two significant sediment types in beaches: finer well-sorted sediments and coarser poorly sorted sediments, where both are coarsely skewed. The finer well-sorted sediment fraction was mainly transported in the seaward and landward directions depending on the wave intensity, while the coarser, poorly sorted sediment generally appeared near the shoreline, which is a highly energetic zone (Gunaratna et al., 2019).

Since Typhoon Rammasun was the most violent typhoon that passed the Beibu Gulf since 1949, the wave caused by the typhoon was considered the most energetic in the past decades. Before Rammasun, the mean grain size of surface sediment at Yintan Beach became finer in the seaward direction, and the very fine sand fraction reached nearly 40% in the lower intertidal zone. Due to the increased wave height superimposed on the tidal level, the very fine sand component of the sediments was washed away by a strong reversing current, especially in the lower intertidal zone, resulting in an obvious erosion in this zone (Figs. 6 and 9). Furthermore, with the rising tidal level, the increase in water depth resulted in a landward shift in the breaking point (Zhang et al., 2014). Such a shift reduced the bottom friction in the previous

depth and amplified the effects of wave action and tidal currents in the subsequent location, inducing a decrease in the very fine sand component and an increase in the fine sand component in the lower intertidal and mid-tidal and swash zone (Fig. 8). In general, the beach experienced retreating in the landward direction in response to the wave action caused by Rammasun.

5.3. Impact of beach morphology

Many studies have claimed the importance of taking the heterogeneous distribution of sediments into consideration to improve the analysis of the coastal morphology (Holland and Elmore, 2008; Gallagher et al., 2011; Jiang et al., 2015), as cross-shore grain size variation was an important factor in the simulation of sediment transport and morphological evolution (Gallagher et al., 1998). In turn, the beach morphology also influences sediment transport and the distribution of grain size characteristics.

Sediment grain size usually differs in various beach morphology units, which related to the hydrodynamic energy environment (Mason and Folk, 1958; Friedman, 1961; Visher, 1969; Stapor and Tanner, 1975). Coarser sediment generally exists in the bar trough and breaking zone where high-energy dissipation happens, while finer sediment is carried away offshore and concentrated elsewhere (Jiang et al., 2015). Based on the classification of Masselink and Short (1993), the dimensionless fall velocity (Ω) of Yintan Beach is 3.3, and the relative tidal range (RTR) is 8.8, which indicates that it is an ultra-dissipative beach (Qi et al., 2010). In contrast to the common patterns of other beaches, the mean grain size of surface sediments at Yintan Beach became finer from the upper beach to lower intertidal zone both before and after Rammasun, and the best sorted sediments were observed in the swash zone where the sandbar was located. This was probably attributed to the beach slope. Before Rammasun, there was a balance between the wave asymmetry-induced net onshore transport and the slope gravity-induced net offshore transport (Dronkers, 2005). Under the high-energy environment of typhoon action, the balance was broken and a larger gradient of the beach slope was formed to reach a new balance (Fig. 5), resulting in very fine sand fraction transport in the lower intertidal and mid-tidal zones.

Comparison of the beach morphology captured by the 3D terrestrial laser scanner at different times showed morphological changes (Fig. 6). The most serious erosion occurred in the lower intertidal zone, with an average erosion intensity of approximately -10 cm, while the most serious accretion was detected in the previous toe of the sandbars, with a peak accretion intensity of approximately 25 cm. Before Rammasun, the sediment grain size and sorting were different in the bar and trough. During Rammasun, waves broke on the bar, and energy was converted via morphological change as a consequence of feedback. The sediments were winnowed in this area and settled down to fill up the toe of the two previous sandbars, which caused the two separate sandbars to turn into one larger sandbar and the swash zone of the beach became flatter after the typhoon. As a consequence, the mean grain size of the sediments in both the previous bar and trough increased, and sediments in this area became better sorted after Rammasun. Apparently, relatively unserious morphological changes can be induced by minor sediment transport with obvious variability in sediment grain size characteristics.

5.4. Impact of wind action

For several decades, Rammasun was the most violent typhoon that impacted Yintan Beach. The severe storm passed over the study area with a maximum wind velocity of 72 m/s and an average wind velocity of approximately 50 m/s. Since the typhoon occurred in the neap tide period, the upper beach around the backshore dune and the berm were still exposed to air even at high tidal levels (Fig. 3a). However, sediment grain size characteristics of the upper beach and berm also changed, where the mean grain size was slightly coarser and the sediments

became better sorted in response to Rammasun, even without hydrodynamic effects. Therefore, strong wind action dominated the variation in the grain size characteristics of the upper beach and berm.

Previous grain size analysis has demonstrated that dune sands that lie in aeolian environments are better sorted and often finer than beach sands (Friedman, 1961; Goldsmith, 1985; Hartmann, 1991). Gallagher et al. (2011) noted that the amount of fine sediment was high in the upper area of the beach, where wind was the main dynamic factor transporting sediment. Pye (1991) concluded that the aeolian sand in northwest England are poorly sorted, while beach sediments are fine-grained and well sorted, by observing the grain size distributions at the beaches and dunes.

In this research, the distribution of sediments in the berm and upper beach is similar to the distribution of sediments at the beach in northwest England (Fig. 7). According to the variations in sediment components before and after Rammasun, the amount of medium sand in the berm and upper beach increased, which was accompanied by a decrease in very fine sand. It could be concluded that during Typhoon Rammasun, the finer particles were selectively transported from the upper beach and berm zone to the foredune where the sand was trapped. The process left a coarser sand component in these two areas, leading to coarse grade and good sorting, eventually resulting in slight erosion in response to wind action.

6. Conclusions

Based on hydrogeomorphological measurements and samples at Yintan Beach before and after Typhoon Rammasun and subsequent laboratory analysis of the sediments, we reveal the changes in the variable pattern of the sediment grain size and identify its potential driving forces. Before Rammasun, the sediment grain size became finer from the upper beach to the lower intertidal zone in the seaward direction. After Rammasun occurred, the sediments were generally coarser, slightly better sorted and with a higher negative skew. The pre-Rammasun grain size pattern mainly had a high content (39%) of very fine sand in the lower intertidal zone. Under the impact of Rammasun, the pattern transformed into a high content (76%) of fine sand in the mid-tidal zone. During Rammasun, wave action was the dominant factor that controlled the main pattern change in the lower intertidal and mid-tidal zones, while the wind action induced slight coarsening of the sediments in the berm and upper beach.

Declaration of competing interest

We declare that we have no financial and personal relationships with other people or organizations that can inappropriately influence our work, there is no professional or other personal interest of any nature or kind in any product, service and/or company that could be construed as influencing the position presented in, or the review of, the manuscript entitled.

Acknowledgements

This study was supported by the National Natural Science Foundation of China (NSFC) (41930537; 41666003; 41866001; 41376097). We gratefully acknowledge Professor Mullarney and the anonymous reviewers for their valuable comments that helped to improve this manuscript.

Appendix A. Supplementary data

Supplementary data to this article can be found online at <https://doi.org/10.1016/j.csr.2019.104006>.

References

- Aagaard, T., Kroon, A., Andersen, S., Sørensen, R.M., Quartel, S., Vinther, N., 2005. Intertidal beach change during storm conditions; Egmond, The Netherlands. *Mar. Geol.* 218, 65–80. <https://doi.org/10.1016/j.margeo.2005.04.001>.
- Abuodha, J.O.Z., 2003. Grain size distribution and composition of modern dune and beach sediments, Malindi Bay coast, Kenya. *J. Afr. Earth Sci.* 36, 41–54. [https://doi.org/10.1016/S0899-5362\(03\)00016-2](https://doi.org/10.1016/S0899-5362(03)00016-2).
- Anonymous, 2013. Optimising the measurement of fine particles. *Met. Powder Rep.* 68, 34–37. [https://doi.org/10.1016/S0026-0657\(13\)70128-0](https://doi.org/10.1016/S0026-0657(13)70128-0).
- Anthony, E.J., 2013. Storms, shoreface morphodynamics, sand supply, and the accretion and erosion of coastal dune barriers in the southern North Sea. *Geomorphology* 199, 8–21. <https://doi.org/10.1016/j.geomorph.2012.06.007>.
- Bascom, W.N., 1951. The relationship between sand size and beach-face slope. *Eos. Trans. AGU* 32 (6), 866–874. <https://doi.org/10.1029/TR0321006p00866>.
- Burvingt, O., Masselink, G., Russell, P., Scott, T., 2017. Classification of beach response to extreme storms. *Geomorphology* 295, 722–737. <https://doi.org/10.1016/j.geomorph.2017.07.022>.
- Conley, D.C., 2003. Cross-shore sediment transport partitioning in the nearshore during a storm event. *J. Geophys. Res.* 108, 3065. <https://doi.org/10.1029/2001JC001230>.
- Costas, S., Alejo, I., Vila-Concejo, A., Nombela, M.A., 2005. Persistence of storm-induced morphology on a modal low-energy beach: a case study from NW-Iberian Peninsula. *Mar. Geol.* 224, 43–56. <https://doi.org/10.1016/j.margeo.2005.08.003>.
- Cox, J.C., Pirrello, M.A., 2001. Applying joint probabilities and cumulative effects to estimate storm-induced erosion and shoreline recession. *Shore Beach* 69 (2), 5–7.
- Dai, Z.-J., Du, J., Zhou, Li, C.C., Chen, Z.S., 2007. The configuration of equilibrium beach profile in South China. *Geomorphology* 86, 441–454. <https://doi.org/10.1016/j.geomorph.2006.09.016>.
- Dai, Z.-J., Chen, J.-Y., Du, J.-Z., Li, C.-C., 2008. Seasonal changes of sandbar behavior in Nanwan beach, south China. *J. Coast. Res.* 245, 1209–1216. <https://doi.org/10.2112/06-0773.1>.
- Dai, Z.-J., Liu, J.T., Lei, Y.-P., Zhang, X.-L., 2010. Patterns of sediment transport pathways on a headland bay beach—Nanwan beach, south China: a case study. *J. Coast. Res.* 26, 1096–1103. <https://doi.org/10.2112/JCOASTRES-D-09-00097.1>.
- Dissanayake, P., Brown, J., Wisse, P., Karunaratna, H., 2015. Comparison of storm cluster vs isolated event impacts on beach/dune morphodynamics. *Estuar. Coast Shelf Sci.* 164, 301–312. <https://doi.org/10.1016/j.ecss.2015.07.040>.
- Dronkers, J., 2005. *Dynamics of Coastal Systems*. Rijkswaterstaat, The Netherlands), p. 21pp.
- Durán, R., Guillén, J., Ruiz, A., Jiménez, J.A., Sagristà, E., 2016. Morphological changes, beach inundation and overwash caused by an extreme storm on a low-lying embayed beach bounded by a dune system (NW Mediterranean). *Geomorphology* 274, 129–142. <https://doi.org/10.1016/j.geomorph.2016.09.012>.
- Friedman, G.M., 1961. Distraction between dune, beach and river sands from their textural characteristics. *J. Sediment. Petrol.* 31, 514–529. <https://doi.org/10.1306/74D70BCD-2B21-11D7-8648000102C1865D>.
- Friedman, G.M., 1967. Dynamic processes and statistical parameters compared for size frequency distribution of beach and river sands. *SEPM J. Sediment. Res.* 37 <https://doi.org/10.1306/74D716CC-2B21-11D7-8648000102C1865D>.
- Friedman, G.M., 1979. Address of the retiring President of the International Association of Sedimentologists: differences in size distributions of populations of particles among sands of various origins. *Sedimentology* 26, 3–32. <https://doi.org/10.1111/j.1365-3091.1979.tb00336.x>.
- Gallagher, E.L., Elgar, S., Guza, R.T., 1998. Observations of sand bar evolution on a natural beach. *J. Geophys. Res.* 103, 3203–3215. <https://doi.org/10.1029/97JC02765>.
- Gallagher, E.L., MacMahan, J., Reniers, A.J.H.M., Brown, J., Thornton, E.B., 2011. Grain size variability on a rip-channelled beach. *Mar. Geol.* 287, 43–53. <https://doi.org/10.1016/j.margeo.2011.06.010>.
- Gallagher, E., Wadman, H., McNinch, J., Reniers, A., Koktas, M., 2016. A conceptual model for spatial grain size variability on the surface of and within beaches. *J. Mar. Sci. Eng.* 4, 38. <https://doi.org/10.3390/jmse4020038>.
- Ge, Z., Dai, Z., Pang, W., Li, S., Wei, W., Mei, X., Huang, H., Gu, J., 2017. LIDAR-based detection of the post-typhoon recovery of a meso-macro-tidal beach in the Beibu Gulf, China. *Mar. Geol.* 391, 127–143. <https://doi.org/10.1016/j.margeo.2017.08.008>.
- Goldsmith, V., 1985. Coastal dunes. In: Davis, R.A. (Ed.), *Coastal Sedimentary Environments*. Springer-Verlag, New York, pp. 171–236.
- Grottole, E., Bertoni, D., Ciavola, P., 2017. Short- and medium-term response to storms on three Mediterranean coarse-grained beaches. *Geomorphology* 295, 738–748. <https://doi.org/10.1016/j.geomorph.2017.08.007>.
- Gunaratna, T., Suzuki, T., Yanagishima, S., 2019. Cross-shore grain size and sorting patterns for the bed profile variation at a dissipative beach: hasaki Coast, Japan. *Mar. Geol.* 407, 111–120. <https://doi.org/10.1016/j.margeo.2018.10.008>.
- Hartmann, D., 1991. Aeolian grain transport. *Acta Mech.* 2, 49–63. <https://doi.org/10.1007/978-3-7091-6703-8>.
- Holland, K.T., Elmore, P.A., 2008. A review of heterogeneous sediments in coastal environments. *Earth Sci. Rev.* 89, 116–134. <https://doi.org/10.1016/j.earscirev.2008.03.003>.
- Huang, H., Dai, Z.J., Shi, W.Y., Sheng, K., 2011. Deposition characteristics of beach profile in strong-tidal environment - a case study of Yintan, Guangxi during spring. *J. Trop. Oceanogr.* 30 (4), 71–76. <http://www.jto.ac.cn/EN/10.11978/j.issn.1009-5470.2011.04.071>.
- Jiang, C., Wu, Z., Chen, J., Deng, B., Long, Y., 2015. Sorting and sedimentology character of sandy beach under wave action. *Procedia Eng.* 116, 771–777. <https://doi.org/10.1016/j.proeng.2015.08.363>.
- Karunaratna, H., Pender, D., Ranasinghe, R., Short, A.D., Reeve, D.E., 2014. The effects of storm clustering on beach profile variability. *Mar. Geol.* 348, 103–112. <https://doi.org/10.1016/j.margeo.2013.12.007>.
- Keijsers, J.G.S., Poortinga, A., Riksen, M.J.P.M., Maroulis, J., 2014. Spatio-temporal variability in accretion and erosion of coastal foredunes in The Netherlands: regional climate and local topography. *PLoS One* 9. <https://doi.org/10.1371/journal.pone.0091115>.
- Lane, E.W., 1947. Report of the subcommittee on sediment terminology. *EOS, Trans. Am. Geophys. Union* 28 (6), 936–938.
- Lee, G., Nicholls J., R., Birkemeier A., W., 1998. Storm-driven variability of the beach nearshore profile at Duck, North Carolina, USA, 1981–1991. *Mar. Geol.* 148, 163–177. [https://doi.org/10.1016/S0025-3227\(98\)00010-3](https://doi.org/10.1016/S0025-3227(98)00010-3).
- Liu, J.T., Zarillo, G.A., 1989. Distribution of grain sizes across a transgressive shoreface. *Mar. Geol.* 87, 121–136. [https://doi.org/10.1016/0025-3227\(89\)90057-1](https://doi.org/10.1016/0025-3227(89)90057-1).
- Loureiro, C., Ferreira, Ó., Cooper, J.A.G., 2012. Geologically constrained morphological variability and boundary effects on embayed beaches. *Mar. Geol.* 329–331. <https://doi.org/10.1016/j.margeo.2012.09.010>, 1–15.
- Mason, C.C., Folk, R.L., 1958. Differentiation of beach, dune, and aeolian flat environments by size analysis, Mustang Island, Texas. *J. Sediment. Petrol.* 28, 211–226. <https://doi.org/10.1306/74D707B3-2B21-11D7-8648000102C1865D>.
- Masselink, G., Kroon, A., Davidson-Arnott, R.G.D., 2006. Morphodynamics of intertidal bars in wave-dominated coastal settings - a review. *Geomorphology* 73, 33–49. <https://doi.org/10.1016/j.geomorph.2005.06.007>.
- Masselink, G., Scott, T., Poate, T., Russell, P., Davidson, M., Conley, D., 2016. The extreme 2013/2014 winter storms: hydrodynamic forcing and coastal response along the southwest coast of England. *Earth Surf. Process. Landforms* 41, 378–391. <https://doi.org/10.1002/esp.3836>.
- Masselink, G., Short, A.D., 1993. The effect of tide range on beach morphodynamics and morphology: a conceptual beach model. *J. Coast. Res.* 9, 785–800. <https://doi.org/10.2307/4298129>.
- McLaren, P., Bowles, D., 1985. The effects of sediment transport on grain-size distributions. *J. Sediment. Res.* 55 (4) <https://doi.org/10.1306/212F86FC-2B24-11D7-8648000102C1865D>.
- McManus, J., 1988. Grain size determination and interpretation. In: Tucker, M. (Ed.), *Techniques in Sedimentology*. Blackwell, Oxford, pp. 63–85.
- Moore, L.J., Benumof, B.T., Griggs, G.B., 1999. Coastal erosion hazards in coastal erosion hazards in santa cruz and san diego counties, California. *J. Coast. Res.* 28, 121–139. <https://doi.org/10.1002/jgrg.20096>.
- Moutzouris, C.I., 1989. Longshore sediment transport rate vs. cross-shore distribution of sediment grain sizes. In: *Coastal Engineering Proceedings*, pp. 1959–1973, 1988.
- Nicholls, R.J., Cazenave, A., 2010. Sea-level rise and its impact on coastal zones. *Science* 328 (5985), 1517–1520. <https://doi.org/10.1126/science.1185782>.
- Otvos, E.G., Beach, W.P., 2004. Beach aggradation following hurricane landfall: impact comparisons from two contrasting hurricanes, northern Gulf of Mexico. *J. Coast. Res.* 20, 326–339.
- Pang, W., Dai, Z., Ge, Z., Li, S., Mei, X., Gu, J., Huang-Hu, 2019. Near-bed cross-shore suspended sediment transport over a meso-macro tidal beach under varied wave conditions. *Estuar. Coast Shelf Sci.* 217, 69–80. <https://doi.org/10.1016/j.ecss.2018.11.007>.
- Pye, K., 1991. Beach deflation and backshore dune formation following erosion under surge conditions: an example from Northwest England. In: *Aeolian Grain Transport*, pp. 171–181.
- Qi, H., Cai, F., Lei, G., Cao, H., Shi, F., 2010. The response of three main beach types to tropical storms in South China. *Mar. Geol.* 275 (1–4), 244–254. <https://doi.org/10.1016/j.margeo.2010.06.005>.
- Russell, P.E., 1993. Mechanisms for beach erosion during storms. *Cont. Shelf Res.* 13, 1243–1265. [https://doi.org/10.1016/0278-4343\(93\)90051-X](https://doi.org/10.1016/0278-4343(93)90051-X).
- Sedrati, M., Anthony, E.J., 2007. Storm-generated morphological change and longshore sand transport in the intertidal zone of a multi-barred macrotidal beach. *Mar. Geol.* 244, 209–229. <https://doi.org/10.1016/j.margeo.2007.07.002>.
- Stapor, F.W., Tanner, W.F., 1975. Hydrodynamic implication of beach, beach ridge and dune grain size studies. *J. Sediment. Petrol.* 45, 926–931. <https://doi.org/10.1306/212F6E88-2B24-11D7-8648000102C1865D>.
- Stockdon, H.F., Doran, K.S., Sallenger, A.H., 2009. Extraction of lidar-based dune-crest elevations for use in examining the vulnerability of beaches to inundation during hurricanes. *J. Coast. Res.* 10053, 59–65. <https://doi.org/10.2112/S153-007.1>.
- Tang, Z., Li, R., Li, X., Jiang, W., Hirsh, A., 2013. Capturing LIDAR-derived hydrologic spatial parameters to evaluate playa wetlands. *J. Am. Water Resour. Assoc.* 50, 234–245. <https://doi.org/10.1111/jawr.12125>.
- Visher, G.S., 1969. Grain-size distributions and depositional processes. *J. Sediment. Petrol.* 39, 1074–1106.
- Ying, M., Zhang, W., Yu, H., Lu, X., Feng, J., Fan, Y.X., Zhu, Y., Chen, D., 2014. An overview of the China meteorological administration tropical cyclone database. *J. Atmos. Ocean. Technol.* 31, 287–301. <https://doi.org/10.1175/JTECH-D-12-00119.1>.
- Zhang, X., Dai, Z., Chu, A., Du, J., 2014. Impacts of relative sea level rise on the shoreface deposition, Shuidong Bay, South China. *Environ. Earth Sci.* 71, 3503–3515. <https://doi.org/10.1007/s12665-013-2740-1>.
- Zhou, G., Huang, J., Yue, T., Luo, Q., Zhang, G., 2015. Temporal-spatial distribution of wave energy: a case study of Beibu Gulf, China. *Renew. Energy* 74, 344–356. <https://doi.org/10.1016/j.renene.2014.08.014>.